

Article

A Tale of 12 Tails: Katanin Severing Activity Affected by Carboxy-Terminal Tail Sequences

K. Alice Lindsay¹, Nedine Abdelhamid¹, Shehani Kahawatte², Ruxandra I. Dima², Dan L. Sackett³, Tara M. Figanegan¹, and Jennifer L. Ross^{1,*}

¹ Physics Department, Syracuse University, Syracuse, New York

² Department of Chemistry, University of Cincinnati, Cincinnati, Ohio

³ Eunice Kennedy Shriver National Institute of Child Health and Human Development, NIH, Bethesda Maryland

* Correspondence: jlross@syr.edu

Abstract: In cells, microtubule location, length, and dynamics are regulated by a host of microtubule-associated proteins and enzymes that read where to bind and act based on the microtubule “tubulin code,” which is predominantly encoded in the tubulin carboxy-terminal tail (CTT). Katanin is a highly conserved AAA ATPase enzyme that binds to the tubulin CTTs to remove dimers and sever microtubules. We have previously demonstrated that short CTT peptides are able to inhibit katanin severing. Here, we examine effects of CTT sequences on this inhibition activity. Specifically, we examine CTT sequences found in nature, alpha1A (TUBA1A), detyrosinated alpha1A, Δ2 alpha1A, beta5 (TUBB/TUBB5), beta2a (TUBB2A), beta3 (TUBB3), and beta4b (TUBB4b). We find that these natural CTTs have distinct abilities to inhibit, most noticeably beta3 cannot inhibit katanin. Two non-native CTT tail constructs are also unable to inhibit – despite having 94% sequence identity with alpha1 or beta5 sequences. Surprisingly, we demonstrate that poly-E and poly-D peptides are capable of inhibiting katanin significantly. An analysis of the hydrophobicity of the CTT constructs indicates that more hydrophobic polypeptides are less inhibitory than more polar polypeptides. These experiments not only demonstrate inhibition, but also likely interaction and targeting of katanin to these various CTTs when they are part of a polymerized microtubule filament.

Keywords: microtubule-severing enzyme; tubulin isotypes; tubulin code; post-translational modifications; katanin; microtubule-associated protein

1. Introduction

Microtubules are essential cytoskeletal structures crucial for cell division, maintaining cellular structure, and intracellular transport. Microtubules are rigid, hollow fibers formed by the polymerization of dimers of two-closely related globular proteins: alpha- and beta-tubulin. Microtubules are highly dynamic and intrinsically grow and shrink in a manner that is known as dynamic instability (reviewed extensively including [1]). Microtubule properties and dynamics are intrinsically differentially regulated by the incorporation of different tubulin isotypes and post-translational modifications. This is known as the ‘tubulin code’ and allows for specialization of microtubules for different functions (reviewed extensively including [2–5]). Microtubule dynamics are also regulated extrinsically by a host of microtubule-associated proteins (MAPs) [6]. MAPs respond to the ‘tubulin code’, which influences their affinity for binding.

Notable amongst MAPs that regulate microtubules is katanin, a conserved AAA ATPase MAP complex that severs and destabilizes microtubules, and consequently regulates cellular homeostasis in a number of different cellular pathways (reviewed in [7,8]). Dysregulation of animal katanin is implicated in developmental, proliferative, and neurodegenerative disorders (reviewed in [9]). Katanin is composed of a 60 kD catalytic subunit (p60), with ATPase and microtubule-severing activities, and a regulatory 80 kD subunit (p80) that regulates the subcellular localization of the complex [10]. Different

oligomerization states of katanin are found [11–13] but like most AAA ATPase enzymes, katanin p60 is active with respect to microtubule severing when in a hexameric ring complex bound to microtubules [14,15]. ATP binding induces hexamerization of the AAA domain and tubulin hydrolysis causes disassembly of the ring complex [10,14]. Human katanin has a poor propensity for oligomerization, which is speculated to prevent aberrant activation and conformation [12].

Katanin regulates microtubule length by both severing and promoting depolymerization [16–19]. Katanin binding and severing on microtubule filaments are separate mechanisms [18,19]. Katanin microtubule regulation is inhibited by 1) sequestration of p60 enzymatic monomer units such that it cannot bind microtubules and 2) posttranslational modifications to p60 [11,18,20–23].







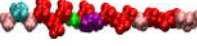
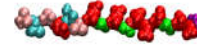



We have previously addressed how microtubules are regulated by katanin by modifying the *in vitro* microtubule severing assay developed [24] to quantify binding of a green fluorescent protein-labeled katanin p60 construct (GFP-kananin) and subsequent severing [18]. Using this assay, we previously demonstrated that adding free tubulin into this assay inhibits the severing action of katanin through competitive and irreversible binding to katanin p60 monomers [18]. Further, short, synthesized peptides with CTT sequences showed the same effect. We have previously found that beta tails are more efficient at inhibiting katanin p60 severing of microtubules in this assay, and therefore that beta CTT sequences more efficiently bind katanin p60.

Here, we examine CTT sequences found in nature, namely alpha1A (TUBA1A), deetyrosinated alpha1A, Δ2 alpha1A, beta5 (formerly called TUBB [25], recently called TUBB5 [26]), beta2a (TUBB2A), beta3 (TUBB3), and beta4b (TUBB4b) [26]. The sequences, charge distributions, and peptide shapes are similar with stretches of negatively charged glutamic acid residues separated by glycine residues (Table 1). The incorporation of hydrophobic residues affects the hydrophobicity of the constructs, as measured using the Wimley-White scale (Table 1) [27]. We find that natural CTTs have distinct abilities to inhibit katanin severing *in vitro*. As previously shown, alpha1A is better at inhibiting than deetyrosinated alpha1A, yet Δ2 alpha1A is better than deetyrosinated alpha1A. While beta5 is still the most potent inhibitor of the beta tails, and beta2a and beta4b are both capable of inhibiting, beta3 is incapable of inhibiting severing by katanin.

These results indicate that the last amino acids are important to the binding and inhibition of CTTs to katanin, so we created two artificial constructs: an alpha1A with the last amino acid (Y) replaced with a phenylalanine and a beta5 construct with the last amino acid (A) replaced with a tyrosine (Table 1). Neither of these two artificial CTT constructs were unable to inhibit – despite having 94% sequence identity with alpha1 or beta5 sequences. Finally, we examined the role of polyglutamylation and charge on the ability to inhibit katanin using constructs with 10 glutamic acids or 10 aspartic acids. Surprisingly, both the poly-E and poly-D peptides are capable of inhibiting katanin significantly. Although this assay examines inhibition, this inhibition is likely caused by competitive binding of the CTTs for the katanin. Thus, these assays provide evidence about which ‘tubulin codes’ can regulate katanin activity in cells.

Table 1. CTT constructs used in this paper showing the name, sequence, total charge, hydrophobicity, and structure. Charge was determined from summing the positive and negative amino acids at pH 7.7. Hydrophobicity was determined using the Wimley-White scale, where a lower number is more hydrophobic and a higher number is less hydrophobic.

Table of Tails

Name	Sequence	Charge	Hydrophobicity	Structure
Alpha1a (TUBA1A/B)	ATADSVEGEGEEEGEEY ATADSV EGEGEEEGEEY	-8	-1.30	
Alpha1-Y (detyrosinated)	ATADSVEGEGEEEGEE ATADSV EGEGEEEGEE	-8	-1.49	
Alpha1-YE (Δ2)	ATADSVEGEGEEEGE ATADSV EGEGEEEGE	-7	-1.40	
Beta5 (TUBB/TUBB5)	ATAEEEEDFGEEAEEEA ATA EEEEDFGEEAEEEA	-10	-1.58	
Beta2a (TUBB2A)	ATADEQGEFEEEEGEDEA ATA DEQGEFEEEEGEDEA	-10	-1.51	
Beta3 (TUBB3)	ATAEEEEEDMYEDDDESEAGGPK ATA EEEEEDMYEDDDESEAGGPK	-11	-1.28	
Beta4b (TUBB4B)	ATAEEEGEFEEEEAEVEA ATA EEEGEFEEEEAEVEA	-10	-1.61	
Alpha1-Y+F	ATADSVEGEGEEEGEEF ATADSV EGEGEEEGEEF	-8	-1.28	
Beta5-A+Y	ATAEEEEDFGEEAEEY ATA EEEEDFGEEAEEY	-10	-1.48	
E10	ATAEEEEEEEEEE ATA EEEEEEEEEE	-10	-2.51	
D10	ATADDDDDDDDDDD ATA DDDDDDDDDD	-10	-1.53	
<div><div>Red: Negatively charged</div><div>Blue: Positively charged</div><div>Cyan: Polar uncharged</div><div>Pink: Hydrophobic</div><div>Purple: Hydrophobic aromatic ring</div><div>Green & Orange: Special cases</div></div>				

2. Materials and Methods

The methods used to purify GFP-katanin and perform the in vitro assays and quantify the data have been previously published [18,19].

Peptides corresponding to the CTT sequences of human tubulins, and modified forms, were custom synthesized and obtained from Peptide 2.0 (Chantilly, VA). Purity and sequence accuracy were confirmed by mass spectrometry performed by Dr. Lisa Jenkins, NCI, NIH.

Complete methods can be found in Appendix A.

3. Results

In this work, we use the *in vitro* microtubule severing assay to quantitatively characterize the microtubule binding and severing ability of human GFP-katanin p60 in the presence of different CTT sequences [18]. First, we ensure that our human GFP-katanin p60 can robustly and reproducibly sever microtubules and completely remove all polymer within 3-5 minutes (Fig. 1A). As each katanin prep has slightly different activity and activity is unstable even when stored at -80°C, each day has a katanin activity control to determine the optimal katanin concentration needed and to serve as a control without added inhibitors (Fig. 1A). For simplicity we use “katanin” to refer to human GFP-katanin p60 for the remainder of this manuscript.

We quantify the intensity of the loss of microtubule polymer and normalize the data to start at 100% (Fig. 1Aii), as previously performed [18]. We also quantify the GFP-katanin binding and normalize the data so that the maximum GFP intensity is one when there are no inhibitors present (Fig1Aiii). As expected, katanin is an ATPase, so it requires

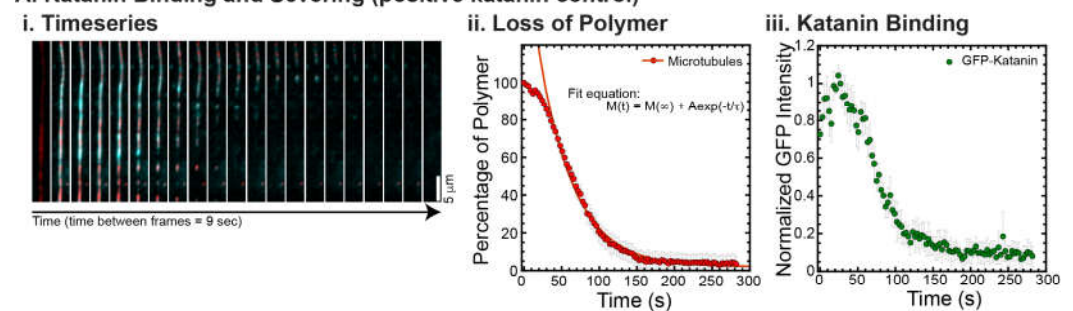
ATP to sever, which we observe (Fig. 1Bi). Without ATP, the loss of polymer is slow (Fig. 1Bii) and appears to be due to depolymerization from filament ends as opposed to severing (Fig. 1Bi). We find that GFP-kananin is still able to bind slowly to microtubules even in the absence of ATP (Fig. 1Bi, iii). This data is normalized to the same day control with katanin and ATP without inhibitor (Fig. 1A) and demonstrates that 70% less GFP-kananin is able to bind in the absence of ATP (Fig. 1Biii).

Katanin has a higher affinity for free tubulin than microtubules and unlike spastin, katanin is inhibited by the presence of tubulin dimers [18,28,29]. We recapitulate that activity (Fig. 1C) and demonstrate that the tubulin dimers inhibit severing and depolymerization (Fig. 1Ci,ii) which is a consequence of the lack of binding (Fig. 1Ci,iii).

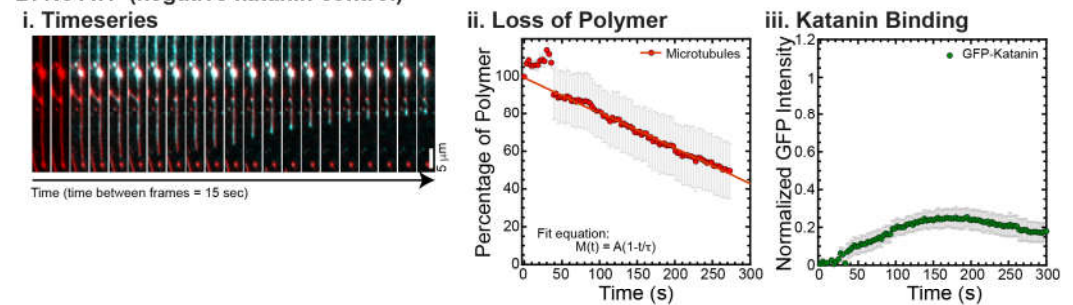
Our previous work using this assay showed that katanin's microtubule severing activity is 1) dependent on katanin p60 concentration; 2) inhibited by free tubulin dimers; and 3) inhibited specifically and differentially by the CTTs of tubulin. Here we use this robust assay to quantitatively interrogate the ability of different tubulin CTT sequences to bind and sequester katanin, and consequently inhibit katanin-microtubule binding and microtubule severing to reveal how the biochemical and biophysical properties of native and non-native CTT sequences, part of the 'tubulin code,' influence katanin-mediated microtubule severing.

Figure 1

A. Katanin Binding and Severing (positive katanin control)



B. No ATP (negative katanin control)



C. Tubulin Dimer Inhibition (positive inhibition control)

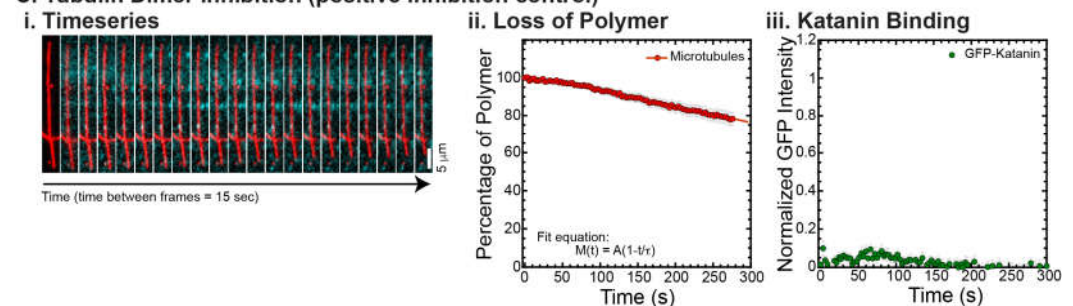


Figure 1. Example data, quantification, and controls. (A) Katanin in the presence of ATP is able to bind and sever microtubules. This daily control demonstrated that katanin was active. (i) Time series of a representative movie showing GFP-kananin binding (cyan) along rhodamine-labeled microtubule (red), becoming severed and losing polymer throughout the filament over time. Scale bar is 5 μm . Time between consecutive frames is 9 s. (ii) Quantification of the loss of polymer measured the signal on the microtubule and the noise 5 pixels away to determine the S/N-1 and then

normalized by the initial time data. Loss of polymer data was fit with an exponential decay equation. Best fit parameters for this data are given in Supplemental Information Table S1. (iii) GFP-katanin binding was quantified in the same way and the S/N-1 was normalized compared to the same day control with ATP (this data), which is why this data has a maximum of 1. (B) Katanin in the absence of ATP is able to bind, although not as well. This daily control demonstrated that katanin ATPase activity was responsible for severing. (i) Time series of a representative movie showing GFP-katanin binding (cyan) along rhodamine-labeled microtubule (red), not severing, but losing polymer from the ends, depolymerizing. Scale bar is 5 μm . Time between consecutive frames is 15 s. (ii) Quantification of the loss of polymer as in part (A). Loss of polymer data was fit with a linear approximation to an exponential decay equation. Best fit parameters for this data are given in Supplemental Information Table S1. (iii) GFP-katanin binding was quantified in the same way and the S/N-1 was normalized compared to the same day control with ATP. (C) Katanin in the presence of ATP and 2 μM tubulin dimers, which inhibit binding and severing. (i) Time series of a representative movie showing GFP-katanin does not bind well (cyan) along rhodamine-labeled microtubule (red). Scale bar is 5 μm . Time between consecutive frames is 15 s. (ii) Quantification of the loss of polymer as in part (A). Loss of polymer data was fit with a linear approximation to an exponential decay equation. Best fit parameters for this data are given in Supplemental Information Table S1. (iii) GFP-katanin binding was quantified in the same way and the S/N-1 was normalized compared to the same day control with ATP. Representative movies in Supplemental Information Movie 1 and 2.

3.1. Katanin Severing Inhibition by Whole Tubulin Dimers, Alpha1a, and Beta5 CTTs

Previously, we showed that free tubulin dimers, alpha1a tubulin CTTs, and beta5 tubulin CTTs can each inhibit katanin severing of microtubules, but there are quantitative differences in the dynamics of katanin binding and rate of microtubule severing [18]. In that prior study, the concentration of CTT was held constant. Here, we vary the amount of alpha1a (TUBA1A/B) or beta5 (TUBB5) CTT from 0 to 2 μM and compare the effects of varying additional tubulin dimers over the same range. We find that, as previously shown, whole tubulin dimers are capable of inhibiting the binding and the severing of microtubules by katanin in a concentration-dependent manner (Fig. 2Ai,Bi). At the highest concentrations of free tubulin (1.5, 2 μM), the amount of katanin binding is not visible above the background level (Fig. 2Bi). Further, at high concentration of free tubulin, the percentage of microtubule polymer over time exhibits a characteristic linear decrease, showing that the loss of polymer is mostly from depolymerization of the filaments - not rapid severing as observed at low tubulin dimer concentrations (Fig 2Ai, best fits given in Supplemental Table S2).

We also showed that beta5 tubulin CTT peptides were better at inhibiting katanin than whole tubulin, while alpha1a tubulin CTTs were not as potent at inhibiting [18]. Indeed, we observe that trend again here, especially at high concentrations of alpha1a and beta5 CTTs (Fig. 2Aii & 2Aiii, best fits given in Supplemental Table S2) where the characteristic decay times are longer at lower beta5 CTT concentrations (Fig 2C). Further, for concentrations where the microtubule polymer is lost, the GFP signal is high as katanin rapidly binds to the microtubules, and then low, due to the loss of polymer to which the katanin binds (Fig. 2Bii, 2D).

Interestingly, for both the beta5 and the alpha1a CTTs at high concentration, the severing is inhibited and initial binding rates for GFP-katanin are significantly lower, but the intensity of GFP-katanin on the filaments increases slowly over time and can reach levels as high as in the absence of CTTs (Fig. 2Bii & iii). Specifically, this can be seen in the GFP katanin plots for alpha1a CTTs at 2 μM (Fig. 2Bii) and beta5 CTTs at 0.5 and 1 μM (Fig. 2Biii).

Qualitatively, it appears that the intensity on the individual microtubules does increase, especially near regions where the microtubule is depolymerizing, as seen in the representative kymograph showing GFP-katanin binding to a microtubule in the presence of 2 μM alpha1a CTT (Fig. 2Ei). This is similar to what is observed in the absence of ATP (Fig. 1B). Quantification of the intensity of GFP-katanin along the microtubule at early, middle, and late times shows that the intensity increases even as some regions reach background levels of intensity due to loss of polymer from the ends or sparse severing events

in the middle of the filament (Fig. 2Eii). Even though there is loss of polymer, the average intensity of GFP-katanin increases, especially compared to the background level measurement, that only shows minor photobleaching (Fig. 2Eiii). Only at the very end, when the microtubule is depolymerizing is there any intensity reduction for the example shown (Fig. 2Eiii), and not all filaments had the same depolymerization in the field (see Supplemental Movie 3, Alpha1a, 2 μ M for the movie).

We previously observed a similar accumulation of katanin at the ends of depolymerizing microtubules lacking the CTT [19]. It is unclear if the accumulation of katanin at tips causes microtubule depolymerization or visa-versa. It could be that the depolymerization of the filaments causes the accumulation of higher concentrations of loosely bound katanin to the ends. Alternatively, it is also possible that the higher accumulation of katanin locally causes the depolymerization of the microtubules. The inhibition caused by high levels of alpha1a and beta5 CTT peptides reduces the rate of katanin binding, while the katanin is still capable of binding and triggering some severing and possibly some depolymerization.

The phenomena of slow accumulation of GFP-katanin without severing was not observed for whole tubulin dimers. Further, previous studies that used CTTs attached to BSA also did not see this accumulation [18]. One major difference between the current study and the previous one is we are using small peptides, while the previous study created constructs that were BSA globular protein with multiple CTTs covalently attached. Further, tubulin dimers also have a globular body attached to the CTTs. The globular domain (BSA or tubulin) could increase the inhibition of the katanin binding and jam the pore of the katanin oligomers, making it difficult for the katanin to bind the microtubules. Conversely, the short CTT peptides we use here that could easily translocate through an oligomer pore, freeing a subset of katanin hexamers to be able to bind to the microtubules.

Taken together, it appears that GFP-katanin binding results in loss of microtubule polymer. Thus, high GFP-katanin binding causes fast severing rates. We calculated the rate from the characteristic decay time using: $r = 1/\tau$ and plotted the severing rate as a function of the measured average, maximum GFP value (Fig. 2F). Apart from the outliers that are high GFP-katanin due to long-time accumulation in the inhibited experiments (denoted in the dashed box), we see a linear relationship between the GFP bound to the microtubules and the rate of loss of polymer. The lines are best fit lines where the accumulation data was excluded to perform the fit (see Supplemental Information Table S3 best fit parameters.)

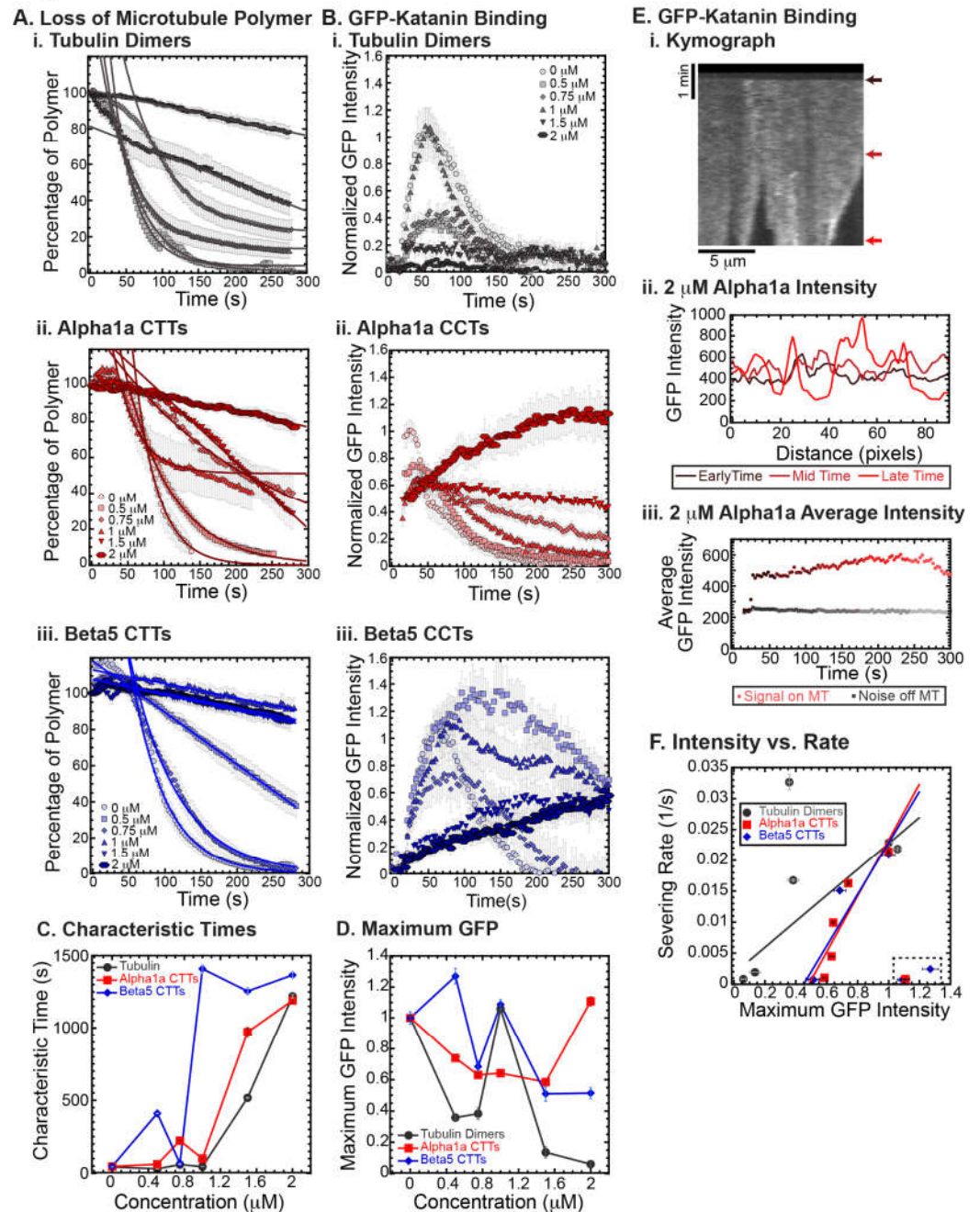
Figure 2

Figure 2. Inhibition of katanin binding and severing by tubulin dimers, alpha CTTs, and beta CTTs. (A) Loss of polymer caused by increasing concentration of (i) tubulin dimers (gray), (ii) alpha CTTs (red), and (iii) beta CTTs (blue). The transition from exponential decay to linear decay is observed for loss of polymer data as it goes from no inhibitor (0 μ M, lightest shade circles), low inhibitor (0.5 μ M, light shade squares; 0.75 μ M, light shade diamonds), medium inhibitor (1 μ M, medium shade triangles with point up), to highest inhibitor (1.5 μ M, darker shade triangles with point down, 2 μ M, darkest shade hexagons). Each data set is fit with a best fit equation to an exponential or linear decay with best fit parameters provided in the Supplemental Information Table S2. (B) The data for the GFP-katanin binding by increasing concentration of (i) tubulin dimers (gray), (ii) alpha CTTs (red), and (iii) beta CTTs (blue). The data was normalized by the maximum when there was no inhibitor (0 μ M, lightest shade circles). Data for low inhibitor (0.5 μ M, light shade squares; 0.75 μ M, light shade diamonds), medium inhibitor (1 μ M, medium shade triangles with point up), to highest inhibitor (1.5 μ M, darker shade triangles with point down, 2 μ M, darkest shade hexagons) are shown. (C) The characteristic decay times for loss of polymer as a function of concentration for tubulin (gray circles), alpha1 CTTs (red squares), and beta CTTs (blue diamonds). Error bars represent the uncertainty in the fit parameters. (D) The average normalized maximum for GFP-katanin

binding to microtubules for tubulin (gray circles), alpha1 CTTs (red squares), and beta CTTs (blue diamonds). Error bars represent the standard deviation of the average. (E) Representative data for GFP-katanin binding in the presence of 2 μ M alpha1 CTT demonstrates the accumulation of GFP-katanin over time is not an artifact. (i) Kymograph of a representative microtubule showing GFP-katanin binding along the microtubule length (horizontal direction, scale bar is 5 μ m of microtubule length) over time (vertical direction, scale bar is 1 min of movie data). Arrows indicate the times used in part ii. (ii) Intensity scans over the microtubule length at early (black line), middle (maroon line), and late (red line) time points indicated in part i show that the intensity fluctuations have increased due to loss of polymer (lowest intensities) and accumulation of GFP-katanin (highest intensities). (iii) Intensity averaged over the length of the microtubule shown in part i plotted over time of the movie for the same region of interest on the microtubule (red circles) and off the microtubule (gray squares) shows that the background intensity is not increasing. (F) Plotting the rate of microtubule severing as a function of average normalized maximum intensity for tubulin (gray circles), alpha1 CTTs (red squares), and beta CTTs (blue diamonds). Data with high GFP-katanin intensity due to a slow accumulation with little loss of polymer denoted by dashed line box (lower right). Removing this data, we fit the severing rate to a linear fit as a function of GFP-katanin. Best fit parameters given in Supplemental Information Table S3. Representative movies in Supplemental Information Movie 2, 3, and 4.

3.2. Katanin Inhibition by Alpha Tail Modifications

A major post-translational modification of tubulin is the detyrosination of the alpha CTT where the final amino acid of the alpha tail, a tyrosine, is removed [2,30,31]. Detyrosinated microtubules can be found among wholly unmodified filaments within the cell. Detyrosination is associated with increased stability to cold treatment in cells [32], but not *in vitro* [33] and reduced binding of destabilizing motor proteins [34]. Further removal of the next amino acid, a glutamic acid, results in a post-translational modification called $\Delta 2$ (Table 1).

We created alpha1a tail constructs with these two modifications and tested their ability to inhibit katanin binding and severing. Both detyrosinated (alpha1a-Y) and $\Delta 2$ (alpha1a-YE) tails were capable of inhibiting katanin, but not as well as full-length alpha1a tubulin CTTs at the highest concentrations (Fig. 3Ai,ii, fit parameters in Supplemental Table S4). Characteristic times increase with increasing CTTs for all with the same trends (Fig. 3C). We quantified the GFP-katanin binding over time (Fig. 3Bi, ii), and found the same trend - full length alpha CTTs inhibited the binding of katanin best, then $\Delta 2$ (alpha-YE) and finally detyrosinated (alpha-Y), which is clear in the data showing the maximum average GFP on the microtubules (Fig. 3D). Based on the data, it appears that alpha CTT is the most active inhibitor, $\Delta 2$ (alpha1a-YE) is the next best, and detyrosinated alpha (alpha1a-Y) is the least effective of the three, although they are all capable of inhibiting binding and severing of katanin at the highest concentrations of CTTs.

Using the GFP-katanin intensity data, we determined the rate for GFP-katanin to associate to the microtubules after being flowed into the chamber (Fig. D). The binding rate is slowest for alpha1a CTTs and the fastest for detyrosinated CTTs with $\Delta 2$ CTTs between (Fig. 3E). The binding rate decrease is occurring for all constructs, but it most apparent for the detyrosinated CTTs. Similar to some of the data observed for alpha1a and beta5 CTTs, the $\Delta 2$ CTTs at the highest concentration (2 μ M), showed the slow binding and leveling off that was observed with alpha CTTs (Fig. 3Bii). The movies revealed the same slow severing and depolymerization observed for alpha1a CTTs (see Supplemental Movie 6).

Finally, we plot the severing rate (inverse of the characteristic severing time) to the maximum amount of GFP bound to the filament (Fig. 3F). Again, we see a linear dependence implying that the severing is directly proportional to the amount of katanin that is able to bind. The boxed region has the data that had a slow GFP-katanin binding rate, but resulted in a high intensity at longer times. This data was excluded from the fit (fit parameters given in Supplemental Information Table S5).

Overall, the effects of the removal of the last few amino acids from the alpha1 tubulin CTT have quantitative and qualitative effects, but the alpha1a peptide is still able to inhibit the binding and severing activity of katanin to similar degrees.

Figure 3

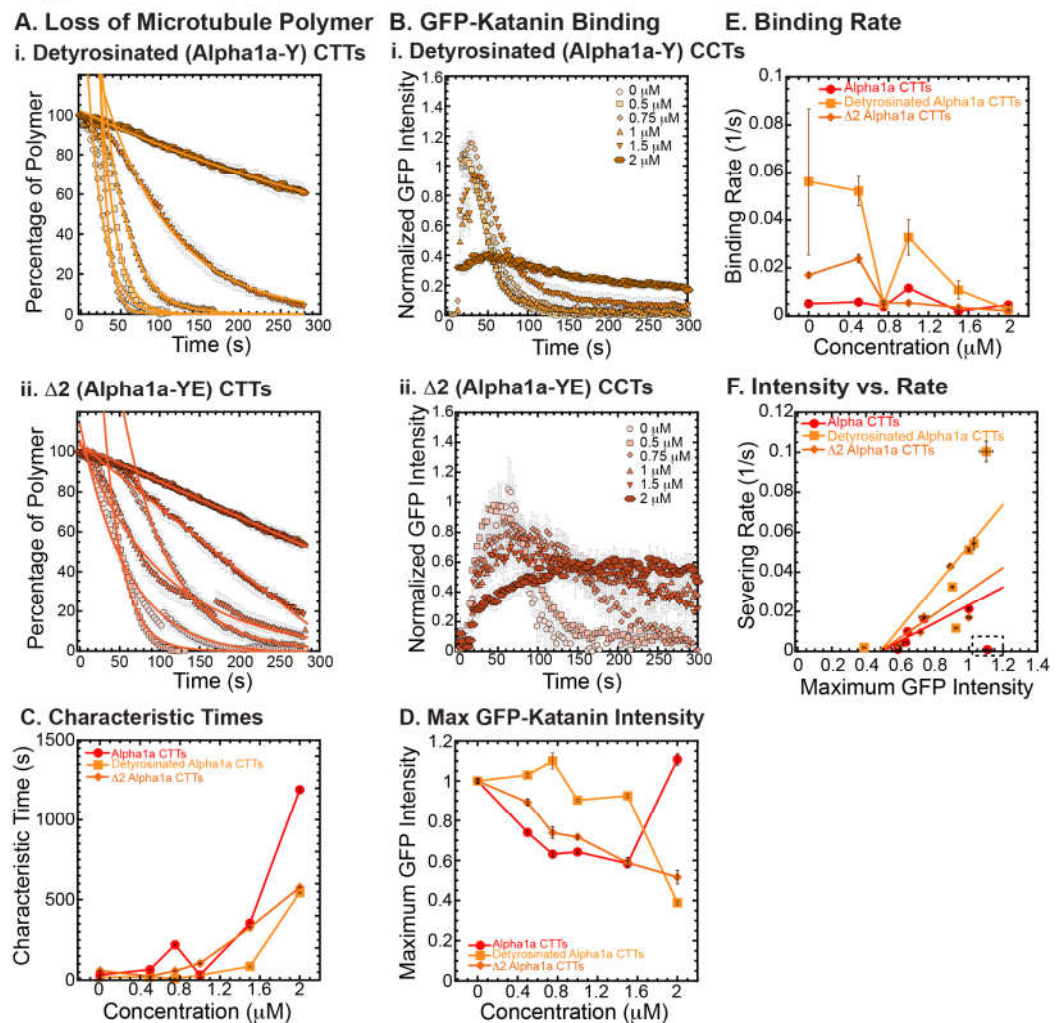


Figure 3. Effects of alpha1a post-translational modifications on katanin inhibition. (A) Loss of polymer caused by increasing concentration of (i) detyrosinated alpha1a CTTs (light orange) and (ii) $\Delta 2$ alpha1a CTTs (dark orange). The transition from exponential decay to linear decay is observed for loss of polymer data as it goes from no inhibitor (0 μM , lightest shade circles), low inhibitor (0.5 μM , light shade squares; 0.75 μM , light shade diamonds), medium inhibitor (1 μM , medium shade triangles with point up), to highest inhibitor (1.5 μM , darker shade triangles with point down, 2 μM , darkest shade hexagons). Each data set is fit with a best fit equation to an exponential or linear decay with best fit parameters provided in Supplemental Information Table S4. (B) The data for the GFP-katanin binding by increasing concentration of (i) detyrosinated alpha1a CTTs (light orange) and (ii) $\Delta 2$ alpha1a CTTs (dark orange). The data was normalized by the maximum when there was no inhibitor (0 μM , lightest shade circles). Data for low inhibitor (0.5 μM , light shade squares; 0.75 μM , light shade diamonds), medium inhibitor (1 μM , medium shade triangles with point up), to highest inhibitor (1.5 μM , darker shade triangles with point down, 2 μM , darkest shade hexagons) are shown. (C) The characteristic decay times for loss of polymer as a function of concentration for alpha1a CTTs (red circles), detyrosinated alpha1a CTTs (light orange squares) and (ii) $\Delta 2$ alpha1a CTTs (dark orange diamonds). Error bars represent the uncertainty in the fit parameters. (D) The average normalized maximum for GFP-katanin binding to microtubules for alpha1a CTTs (red circles), detyrosinated alpha1a CTTs (light orange squares) and (ii) $\Delta 2$ alpha1a CTTs (dark orange diamonds). Error bars represent the standard deviation of the average. (E) GFP-katanin binding was measured for the initial time points for each data set by fitting a linear fit equation from the initial times to the time when maximum is reached. The slopes of the fits represent the rate of katanin binding, plotted as a function of CTT concentration for alpha1a CTTs (red circles), detyrosinated alpha1a CTTs (light orange squares) and (ii) $\Delta 2$ alpha1a CTTs (dark orange diamonds). Error bars represent the uncertainty in the fit parameters. (F) Plotting the rate of microtubule severing as a function of average normalized maximum intensity for alpha1a CTTs (red circles), detyrosinated alpha1a CTTs (light orange squares) and (ii) $\Delta 2$ alpha1a CTTs (dark orange diamonds). Data with

high GFP-katanin intensity due to a slow accumulation with little loss of polymer denoted by dashed line box (lower right). Removing this data, we fit the severing rate to a linear fit as a function of GFP-katanin, provided in Supplemental Information Table S5. Representative movies in Supplemental Information Movies 5 and 6.

3.3. Katanin Inhibition by Beta Tail Isootypes

Beta tubulin isotype CTTs are more diverse in their sequence differences compared to alpha isotype CTTs (Maleikal 2022). Here, we examine some of the most diverse tails to determine if they have different abilities to inhibit katanin. Specifically, we examine beta2a (TUBB2A), beta3 (TUBB3), and beta4b (TUBB4B), which we compare to beta5 (TUBB5) (Table 1).

Examining beta2a CTTs, the sequence is not so dissimilar from beta5 (Table 1). The most striking difference is the disruption of a chain of repeating glutamic acids with a glycine and the addition of a glutamate and a glycine closer to the amino-terminus of the peptide. These subtle differences are enough to shift the inhibition concentration, so that more beta2a is needed to inhibit katanin binding and severing compared to beta5 CTTs (Fig. 4Ai, C, best fits are given in Supplemental Information Table S6). Along with the loss of severing is the same reduction in GFP-katanin binding (Fig. 4Bi, D).

The beta3 CTTs are the most unusual in terms of sequence, with various unique residues at the end ending with a positively charged lysine. We find that beta3 CTTs cannot inhibit katanin severing (Fig. 4Aii, best fits are given in Supplemental Information Table S6). Further, there is little inhibition of GFP-katanin binding (Fig. 4Bii). Despite the quantitative reduction of severing rate and binding, for the two highest concentrations of beta3 CTT (1.5 and 2 μ M), the movies qualitatively show clear and rapid severing of microtubules even at 2 μ M beta3 CTT (see Supplemental Movie 8). Beta3 cannot inhibit katanin binding or severing activity.

Beta4b CTT's sequence is more canonical than beta3 except the presence of a valine with the alanine at the very end of the peptide. These residues are uncharged and hydrophobic, which could affect interactions with katanin. We find that beta4b CTTs are able to inhibit katanin severing (Fig. 4Aiii, best fits are given in Supplemental Information Table S6) and binding (Fig. 4Biii), although to a lesser extent than beta or beta2a CTTs (Fig. 4A,C). Linear fits to the severing rate plotted against the maximum GFP intensity show the same linear dependence (Fig. 4E, best fits given in Supplemental Information Table S7).

The sequence of the CTT appears to have a significant impact with the peptides ability to interact with and inhibit katanin. From the beta CTT tail data, it appears that relatively small changes that are naturally occurring can have large impacts on interactions (Fig. 4). Interestingly, for both the alpha and beta tails tested, changes to the end of the CTT construct have impacts on katanin interactions (Figs. 3, 4).

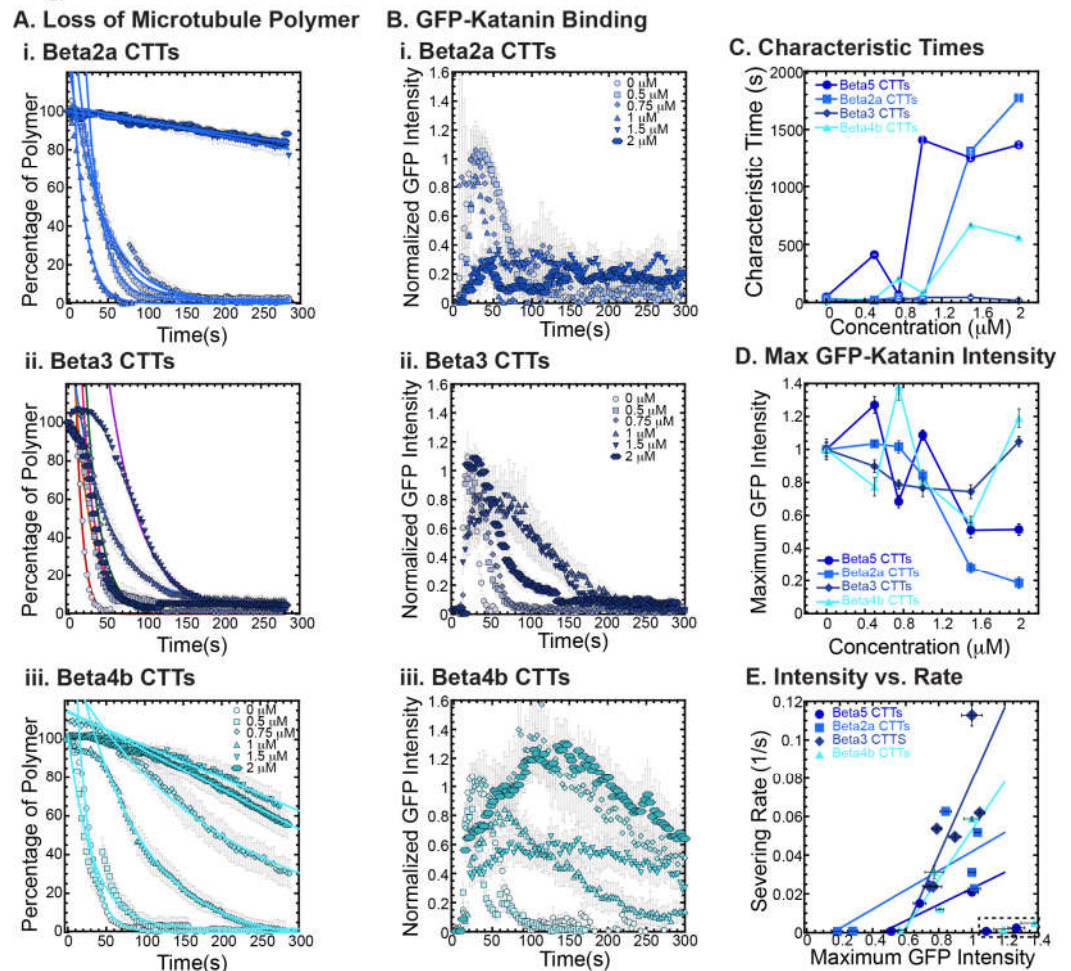
Figure 4

Figure 4. Effects of beta tubulin isotype sequence on katanin inhibition. (A) Loss of polymer caused by increasing concentration of (i) beta2a CTTs (light blue), (ii) beta3 CTTs (navy blue), and (iii) beta4b CTTs (cyan). The transition from exponential decay to linear decay is observed for loss of polymer data as it goes from no inhibitor (0 μM , lightest shade circles), low inhibitor (0.5 μM , light shade squares; 0.75 μM , light shade diamonds), medium inhibitor (1 μM , medium shade triangles with point up), to highest inhibitor (1.5 μM , darker shade triangles with point down, 2 μM , darkest shade hexagons). Each data set is fit with a best fit equation to an exponential or linear decay with best fit parameters provided in Supplemental Information Table S6. (B) The data for the GFP-katanin binding by increasing concentration of (i) beta2a CTTs (light blue), (ii) beta3 CTTs (navy blue), and (iii) beta4b CTTs (cyan). The data was normalized by the maximum when there was no inhibitor (0 μM , lightest shade circles). Data for low inhibitor (0.5 μM , light shade squares; 0.75 μM , light shade diamonds), medium inhibitor (1 μM , medium shade triangles with point up), to highest inhibitor (1.5 μM , darker shade triangles with point down, 2 μM , darkest shade hexagons) are shown. (C) The characteristic decay times for loss of polymer as a function of concentration for beta CTTs (bright blue circles), beta2a CTTs (light blue squares), beta3 CTTs (navy blue diamonds), and beta4b CTTs (cyan triangles). Error bars represent the uncertainty in the fit parameters. (D) The average normalized maximum for GFP-katanin binding to microtubules for beta CTTs (bright blue circles), beta2a CTTs (light blue squares), beta3 CTTs (navy blue diamonds), and beta4b CTTs (cyan triangles). Error bars represent the standard deviation of the average. (E) Plotting the rate of microtubule severing as a function of average normalized maximum intensity for beta CTTs (bright blue circles), beta2a CTTs (light blue squares), beta3 CTTs (navy blue diamonds), and beta4b CTTs (cyan triangles). Data with high GFP-katanin intensity due to a slow accumulation with little loss of polymer denoted by dashed line box (lower right). Removing this data, we fit the severing rate to a linear fit as a function of GFP-katanin. Representative movies in Supplemental Information Movies 7, 8, and 9.

3.4. Examination of Katanin Inhibition by Artificial CTTs where the Last Amino Acid is Altered

As demonstrated above for the alpha and beta CTTs, the tail sequence – especially the last amino acid – can impact the interaction and inhibition activity on katanin's binding and severing ability. Here, we investigate that effect by creating two artificial tail constructs, one based on alpha1a and one based on beta5, to determine the impacts of a change just to the very c-terminus of the peptide sequence. The two constructs we created are named alpha1a-Y+F and beta5-A+Y.

For the alpha1a-Y+F CTT, removing the final tyrosine and adding a phenylalanine residue to the very end of the alpha CTT should not significantly change the size or charge of the peptide, since tyrosine and phenylalanine are only different by the addition of an OH group on the carbon ring. Yet, the changing of the final amino acid on alpha1a has major consequences to katanin binding and severing. The alpha1a-Y+F CTT has no inhibitory effect on GFP-katanin severing (Fig. 5Ai, best fits given in Supplemental Information Table S8) or binding (Fig. Bi). This one seemingly minor change demonstrates the importance of the final residue to the activity of the alpha1a CTTs in their interaction with katanin. The severing rates appear linear with respect to the GFP-katanin binding (Fig. 5E, see Supplemental Information Table S9 for best fits).

The alpha1a data implies that the final amino acid being a tyrosine is very important for GFP-katanin inhibition. The beta5 CTT is the most potent inhibitor of the CTTs we tested. In order to determine if the tyrosine will enhance the inhibition caused by beta5, we created an artificial beta5-A+Y construct where we remove the final alanine and replace it with a tyrosine. Surprisingly, we find that this construct is far less potent as a katanin inhibitor (Fig. 5Aii, best fits given in Supplemental Information Table S8) and does not affect katanin binding (Fig. 5Bii). This result again confirms the importance of the final residue and indicates that the tyrosine is not optimized for the beta5's interaction with katanin, and instead completely eliminates the interaction.

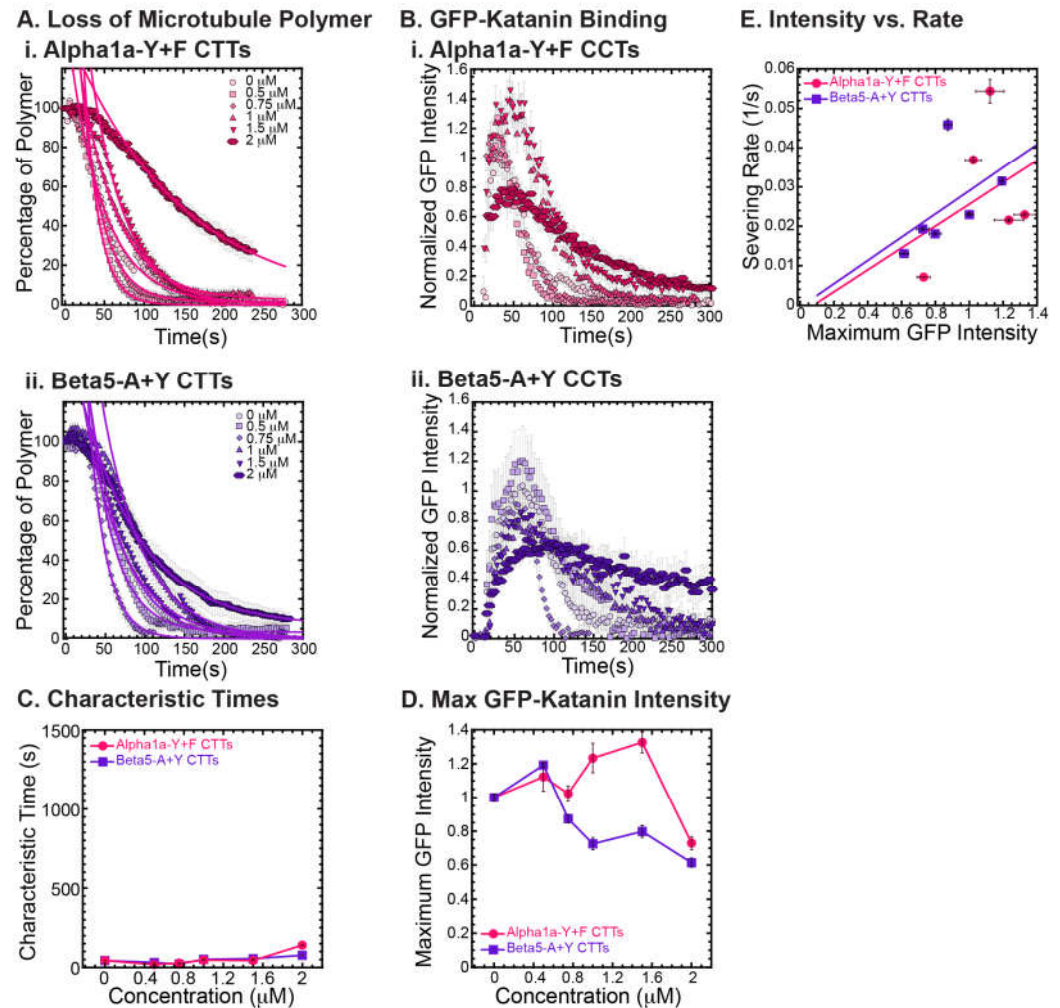
Figure 5

Figure 5. Katanin severing and binding not inhibited by artificially constructed CTTs. (A) Loss of polymer caused by increasing concentration of (i) alpha-Y+F CTTs (magenta) and (ii) beta-A+Y CTTs (purple). All data sets were fit to exponential decays because these CTTs did not inhibit severing significantly as the amount of inhibitor is changed from no inhibitor (0 μM , lightest shade circles), low inhibitor (0.5 μM , light shade squares; 0.75 μM , light shade diamonds), medium inhibitor (1 μM , medium shade triangles with point up), to highest inhibitor (1.5 μM , darker shade triangles with point down, 2 μM , darkest shade hexagons). Each data set is fit with a best fit equation to an exponential with best fit parameters provided in Supplemental Information Table S8. (B) The data for the GFP-katanin binding by increasing concentration of (i) alpha-Y+F CTTs (magenta) and (ii) beta-A+Y CTTs (purple). The data was normalized by the maximum when there was no inhibitor (0 μM , lightest shade circles). Data for low inhibitor (0.5 μM , light shade squares; 0.75 μM , light shade diamonds), medium inhibitor (1 μM , medium shade triangles with point up), to highest inhibitor (1.5 μM , darker shade triangles with point down, 2 μM , darkest shade hexagons) are shown. (C) The characteristic decay times for loss of polymer as a function of concentration for alpha-Y+F (magenta circles) and beta-A+Y CTTs (purple squares). Error bars represent the uncertainty in the fit parameters. (D) The average normalized maximum for GFP-katanin binding to microtubules for alpha-Y+F (magenta circles) and beta-A+Y CTTs (purple squares). Error bars represent the standard deviation of the average. (E) Plotting the rate of microtubule severing as a function of average normalized maximum intensity for alpha-Y+F (magenta circles) and beta-A+Y CTTs (purple squares). No data displayed high GFP-katanin intensity due to a slow accumulation with little loss of polymer denoted by dashed line box (lower right). All data of the severing rate was fit to a linear function of GFP-katanin (see Supplemental Information Table S9 for best fits). Representative movies in Supplemental Information Movies 10 and 11.

3.4. Katanin Inhibition by Poly-E and Poly-D peptides

One major similarity between alpha and beta CTTs is that there are repeats of glutamic acids within the sequence for both. Further, there is an additional post-translational modification that can occur on both the alpha and beta CTTs of polyglutamylation, where multiple branched poly-E peptides can be attached to residue 445 of alpha1a or beta2A or beta3 at residue 435 and 438, respectively [2,5,23]. Thus, poly-E peptides may alter the interactions of the tubulin CCTs with associated enzymes and proteins.

To test if poly-E peptides can interact with and inhibit katanin, we created a non-native CTT sequence composed of 10 glutamic acid residues in a row (10E). We also made a 10 amino acid sequence of aspartic acid (D10) to test amino acid specificity using another residue that is also charged. The D10 construct has the same charge as the E10, but has a slightly modified structure. Although no poly-aspartic acid chains are post-translationally modified on tubulin, there are regions of the naturally occurring alpha and beta CTTs that have aspartic acids instead of glutamic acids.

We find that both the E10 and the D10 sequences can inhibit the severing activity (Fig. 6A, best fits given in Supplemental Information Table 10) and binding of GFP-katanin (Fig. 6B). Interestingly, despite having no specific CTT sequence, the E10 and D10 inhibition activity follows a similar trend in inhibition of characteristic times, specifically, they inhibit best at the higher concentrations (Fig. 6C, 1.5 and 2 μ M). These two concentrations also have significantly reduced katanin binding rates and maximum binding intensities (Fig. 6D). The linear dependence on severing rate as a function of GFP-katanin binding is better for D10 compared to E10 (Fig. 6E, best fits given in Supplemental Information Table S11). The fact that poly-E and poly-D peptides can inhibit katanin severing is surprising considering that these constructs are not CTTs. They do not have the interspersed uncharged residues and are not ended with a hydrophobic residue as the other constructs are. The katanin inhibition of these two constructs imply that negative charge is a likely driver for the interaction with katanin.

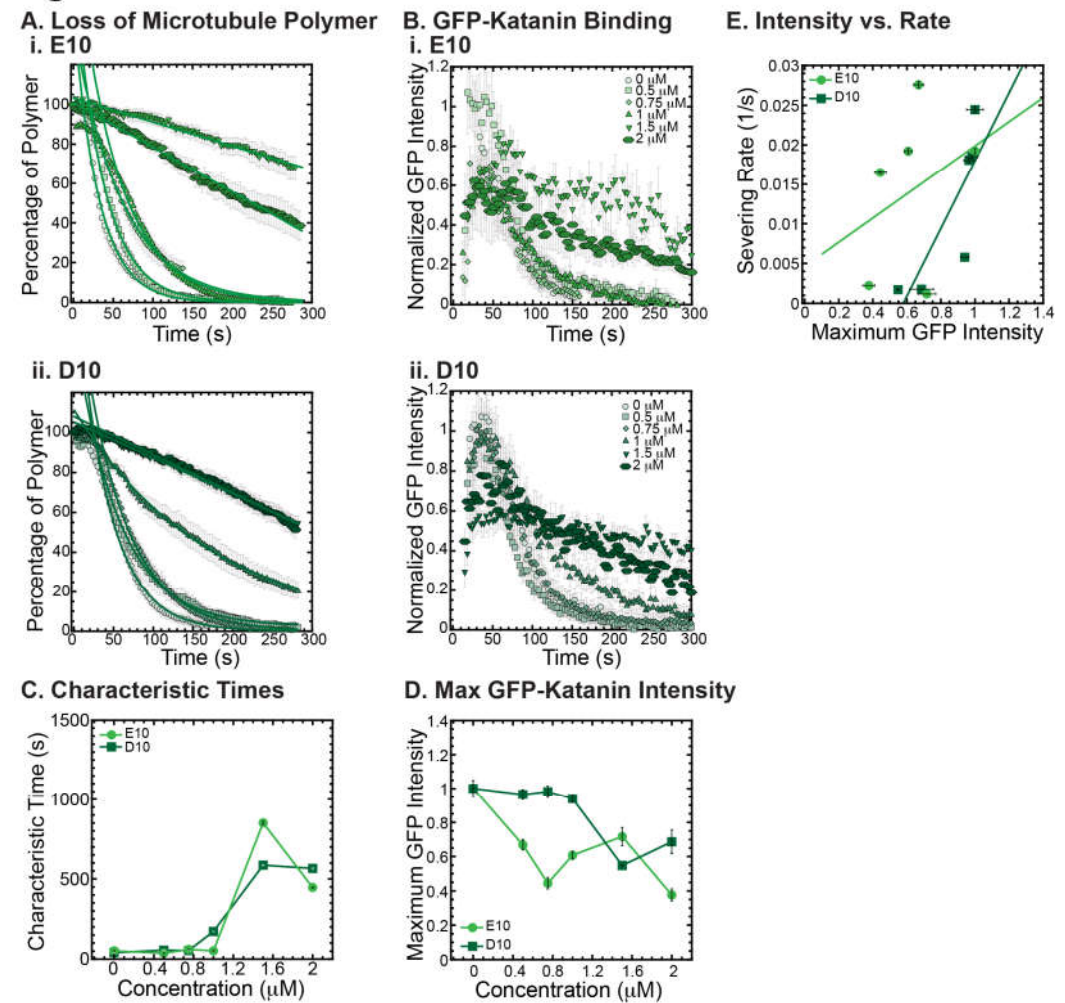
Figure 6

Figure 6. Katanin severing and binding inhibited by poly-E and poly-D peptides. (A) Loss of polymer caused by increasing concentration of (i) E10 peptides (light green) and (ii) D10 peptides (dark green). Data sets were fit to exponential decays because these CTTs did not inhibit severing significantly as the amount of inhibitor is changed from no inhibitor (0 μM , lightest shade circles), low inhibitor (0.5 μM , light shade squares; 0.75 μM , light shade diamonds), medium inhibitor (1 μM , medium shade triangles with point up), to highest inhibitor (1.5 μM , darker shade triangles with point down, 2 μM , darkest shade hexagons). The transition from exponential decay to linear decay is observed for loss of polymer data as it goes from no inhibitor (0 μM , lightest shade circles), low inhibitor (0.5 μM , light shade squares; 0.75 μM , light shade diamonds), medium inhibitor (1 μM , medium shade triangles with point up), to highest inhibitor (1.5 μM , darker shade triangles with point down, 2 μM , darkest shade hexagons). Each data set is fit with best fit equation provided in Supplemental Information Table S10. (B) The data for the GFP-katanin binding by increasing concentration of (i) E10 peptides (light green) and (ii) D10 peptides (dark green). The data was normalized by the maximum when there was no inhibitor (0 μM , lightest shade circles). Data for low inhibitor (0.5 μM , light shade squares; 0.75 μM , light shade diamonds), medium inhibitor (1 μM , medium shade triangles with point up), to highest inhibitor (1.5 μM , darker shade triangles with point down, 2 μM , darkest shade hexagons) are shown. (C) The characteristic decay times for loss of polymer as a function of concentration for E10 peptides (light green circles) and D10 peptides (dark green squares). Error bars represent the uncertainty in the fit parameters. (D) The average normalized maximum for GFP-katanin binding to microtubules for E10 peptides (light green circles) and D10 peptides (dark green squares). Error bars represent the standard deviation of the average. (E) Plotting the rate of microtubule severing as a function of average normalized maximum intensity for E10 peptides (light green circles) and D10 peptides (dark green squares). No data displayed high GFP-katanin intensity due to a slow accumulation with little loss of polymer denoted by dashed line box (lower right). All data of the

severing rate was fit to a linear function of GFP-katanin (see Supplemental Information Table S11). Representative movies in Supplemental Information Movies 12 and 13.

4. Discussion

We used an *in vitro* microtubule severing assay we developed previously with purified GFP-katanin to interrogate if the CTT sequence of tubulin regulates inhibition of katanin microtubule severing [18]. These studies are important to understand the ability of different microtubule substrates to be severed by katanin. Although we are using an inhibition assay, the inhibition is mediated by the ability of the severing enzyme to bind to the CTT introduced. If there is significant inhibition by a CTT sequence, this indicates that there is a good interaction of katanin for that sequence - good enough to compete with the microtubule substrate present. For sequences that are good inhibitors, we interpret that the same sequence, when part of a tubulin dimer incorporated into a microtubule, will also be a good substrate for katanin. Thus, all the good inhibitors are likely good targets for katanin degradation. Poor inhibitors are likely poor targets for katanin interaction and degradation.

A recent study has shown that microtubules with post-translational modifications do display different abilities for katanin binding and severing [23]. Many of the trends we report here for inhibition are also observed for microtubules made with post-translationally modified tubulins. Specifically, they observe that poly-glutamylation of alpha tails results in more binding and severing whereas polyglutamylation of beta tails is biphasic with more binding, but non-monotonic increase than decrease in severing activity [23]. Our results with poly-E peptides also predict the same increased binding interaction they observe. They also find that detyrosination of the alpha tails results in decreased binding and severing activity [23], as we also observe with our CTTs.

We find that alpha, beta, modified alphas (detyrosinated and $\Delta 2$), and some beta isoforms are moderate to good targets for katanin. Perhaps more intriguing are the poor targets. Beta3 tubulin is a poor target for katanin. Beta3 isoforms are found in brain nerve cells - specifically expressed in the axons and dendrites [35]. Mutants of beta3 result in impairment of vision and large-scale brain structure deformations that can result in neurological defects [36]. It also appears to be important for nerve cell regrowth [37]. It is interesting that such an important isoform is not a target for katanin. It is known that katanin defects also result in poor development of the brain - specifically causing microcephaly and lissencephaly [38–40]. Interestingly, there is no overlap in the structures or phenotypes between katanin mutations or deletion phenotypes and beta3 deletion or mutation phenotypes - implying that they likely do not interact with each other, despite being both important required proteins for brain development.

Perhaps surprisingly, deetyrosinated alpha1a is still capable of inhibiting katanin, implying it is a moderate good target for katanin degradation. Detyrosination is associated with stability of microtubules in cells [32]. Yet, *in vitro* reconstitution of deetyrosinated microtubules shows that stability is not conferred directly from the deetyrosination [33]. Thus, it is most likely that deetyrosination is a signal to destabilizing elements to avoid these microtubules. It has been shown that deetyrosinated microtubules are avoided by MCAK, a depolymerizing kinesin [34]. Here, we show some reduced affinity of katanin with deetyrosinated alpha CTTs, but not so significant to imply it could not be degraded by katanin.

The other constructs that were poor targets were the non-native peptides we made from alpha1a and beta5. These constructs demonstrate that the importance of the last amino acid in the sequence for both the alpha and beta sequences. It was surprising that the phenylalanine had such a drastic effect, given the similarities between it and tyrosine. Further, if tyrosine is so important, why is the beta tail sequence with a tyrosine attached as the last residue such a poor inhibitor? To add to our surprise, we found that two constructs with poly-E or poly-D inhibited katanin just as well as native tails. The E10 construct is like polyglutamylation post-translational modification that can occur on alpha or beta tails.

We have found that katanin activity is sensitive to the pH of the solution. Specifically, katanin is completely inhibited at pH 6.6 (Supp. Fig. 1). It prefers a higher pH closer to 8, and we use pH 7.7 in our assays because microtubules prefer a slightly acidic buffer (PEM is a PIPES buffer with pH 6.8). If the addition of the E10 or the D10 constructs could change the pH, that could be the cause of the inhibition. We calculate that, for the highest concentration of D10 or E10, the pH would only shift by 0.01 - not enough to cause the deactivation of katanin due to pH. Thus, we believe that inhibition is truly caused by the D10 and E10 peptides interacting with katanin directly. Future works examining the interaction using other techniques may reveal the binding affinity of these unnatural tail sequences.

On interesting aspect of the CTTs is that they are all negatively charged (Table 1), but apart from being negative, there does not seem to be a correlation between their activity and their overall charge. For instance, the beta3 CTT has a total charge of -11, but it is a poor inhibitor of katanin. Instead, we focus on another biochemical and biophysical aspect of the CTTs – their hydrophobicity. Based on the recent findings from the literature [41], we evaluated the hydrophobicity of the peptides using the Wimley-White scale [27], which represents the free energy change when transferring pentapeptides between water and a lipid bilayer. This scale was shown to perform very well in several experimental and computational tests, compared to the more traditional scales, such as the Kyte-Doolittle scale [41]. For each of the 11 peptides tested in our work, we calculated their average hydrophobicity (the total hydrophobicity of the peptide divided by its length) in order to compare directly peptides of different lengths (Table 1).

As discussed above and in the literature [33], alpha and beta-tubulin tails interact differently with katanin. Alpha-tails have a preferred interaction outside of the AAA core of the motor, while the beta-tails interact directly with the ATPase domain by contacting the pore loops of the protomers in the hexameric states of the motor. We used the data from Table 1 to rank order the alpha peptides and the beta peptides separately.

We found that the synthetic alpha1a-Y+F peptide is the most hydrophobic of the 5 alpha tails, followed by the alpha1a, and alpha1-YE, with alpha1-Y being the most hydrophilic. For the beta tails, we found that beta3 is the most hydrophobic peptide, followed by beta5-A+Y, beta2a, beta5, and finally beta4. The two acidic peptides, D10 and E10 are highly polar, with E10 being the most polar of the 11 peptides.

Although the hydrophobicity trends do not exactly replicate the trends we observe, there is a much better correlation than the total charge. As example, for both alpha and beta tails, the most hydrophobic peptides are unable to inhibit katanin severing. In contrast, more polar peptides inhibit severing by katanin. Namely, the two synthetic peptides built from the alpha1a and the beta5 CTTs are more hydrophobic than the corresponding wild-type tails. Beta3 is the most hydrophobic of all beta CTTs. These are the 3 tubulin tails that are unable to inhibit severing. Even for beta2a, which is more hydrophobic than beta5, we found that it needs higher concentration, compared to beta5, to inhibit severing. We also note that beta5 is a better inhibitor of katanin severing than alpha1a, which correlates with the fact that alpha1a is more hydrophobic than beta5. For more hydrophilic peptides, such as alpha1a-Y, we found a decrease in katanin microtubule binding and severing, which has been reported also by a recent study [23], indicating that more hydrophilic tails are good inhibitors of katanin binding and severing of microtubules. Finally, we note that among the human alpha tubulins, alpha8, which plays a critical role in cortical progenitor differentiation [33], is the only tail with a C-terminal F. This tail has the sequence DSFEENEAGEEF resulting in an average hydrophobicity of -1.20, which makes it the most hydrophobic of all the tails. Based on our results, especially the synthetic alpha1a-Y+F tail, we predict that the presence of phenylalanine at the end of an alpha-tail increases its hydrophobicity, compared to the wild-type alpha1a, and will make it unable to inhibit katanin severing.

Analysis of the hydrophobicity of the peptides shows that for both alpha and beta CTTs, any change that increases the average hydrophobicity of the peptide leads to a reduced or complete loss in the ability to inhibit katanin severing. In addition, peptides characterized by high hydrophilicity inhibit severing more readily than hydrophobic

ones, which explains the inhibitory effect of the poly-D and poly-E tails. We note that the results of the hydrophobicity analysis are robust even at the more basic pH used in our experiments, as the differences between the behavior of the peptide tails are due to the amino acid types that have been shown to have hydrophobicity values independent of pH over a large interval [42].

5. Conclusions

The new experimental results described here support the tubulin code model for how MAPs and microtubule-enzymes can be directed to act in time and space by the sequence and post-translational modifications to tubulin's CTT. Future screens of this sort can be used to make predictions about which tubulin isotypes are good or poor targets for degradation by katanin. Katanin activity has also been linked to downstream increasing of microtubule networks and enhanced stability of individual filaments [29,43,44]. Thus, these experiments will also predict which tissues expressing different isotypes might have less dense microtubule networks or less stable filaments. Future *in vitro* experiments with different tails, modified tubulins as microtubules, and even expressing different isotypes in live cells will be needed to address the predictions from this work.

Supplementary Materials: Table S1: Loss of microtubule polymer fits for data in Figure 1; Table S2: Loss of microtubule polymer fits for data in Figure 2; Table S3: Severing Rate vs. Maximum GFP Intensity for data in Figure 2F. Fits to a linear fit equation: $y = mx + b$; Table S4: Loss of microtubule polymer fits for data in Figure 3; Table S5: Severing Rate vs. Maximum GFP Intensity for data in Figure 3F. Fits to a linear fit equation: $y = mx + b$; Table S6: Loss of microtubule polymer fits for data in Figure 4; Table S7: Severing Rate vs. Maximum GFP Intensity for data in Figure 4D. Fits to a linear fit equation: $y = mx + b$; Table S8: Loss of microtubule polymer fits for data in Figure 5; Table S9: Severing Rate vs. Maximum GFP Intensity for data in Figure 5E. Fits to a linear fit equation: $y = mx + b$; Table S10: Loss of microtubule polymer fits for data in Figure 6; Table S11: Severing Rate vs. Maximum GFP Intensity for data in Figure 6E. Fits to a linear fit equation: $y = mx + b$; Figure S1: pH affects katanin activity; Table S12: Loss of microtubule polymer fits for data in Supplemental Figure 1; Supplemental Movie 1: Controls.avi; Supplemental Movie 2: Tubulin.avi; Supplemental Movie 3: Alpha1.avi; Supplemental Movie 4: Beta5.avi; Supplemental Movie 5: Alpha1-Y.avi; Supplemental Movie 6: Alpha1-YE.avi; Supplemental Movie 7: Beta2a.avi; Supplemental Movie 8: Beta3.avi; Supplemental Movie 9: Beta4b.avi; Supplemental Movie 10: Alpha1-Y+F.avi; Supplemental Movie 11: Beta5-A+Y.avi; Supplemental Movie 12: E10.avi; Supplemental Movie 13: D10.avi.

Author Contributions: Conceptualization, JLR and DS; methodology, JLR and DS; validation, KAL, NA and JLR; formal analysis, KAL, NA, and JLR; investigation, KAL, JLR, NA, TMF; resources, KAL; data curation, KAL and JLR; writing—original draft preparation, JLR, TMF, KAL, and NA; writing—review and editing, JLR, TMF, KAL, DS, RID; visualization, SK, RID, and JLR; supervision, RID, DS, KAL, and JLR; project administration, JLR and DS; funding acquisition, DS, RID and JLR. All authors have read and agreed to the published version of the manuscript.

Funding: KAL, NA, and JLR were funded by research grant from the National Institutes of Health NIH 1R15GM141722. SK and RID were funded by research grant from the National Science Foundation NSF MCB-1817948. This work was also supported by the Intramural Research Program of the Eunice Kennedy Shriver National Institute of Child Health and Human Development, NIH, Bethesda, Maryland.

Institutional Review Board Statement: Not applicable.

Informed Consent Statement: Not applicable.

Data Availability Statement: Microscopy data reported in this paper will be shared by the corresponding author upon request. This paper does not use any original code.

Acknowledgments: We wish to thank Dr Lisa Jenkins (NCI, NIH) for help with Mass Spectrometry confirmation of the synthesized peptides. We would like to thank the Ross Lab members for regular feedback on this work.

Conflicts of Interest: The authors declare no conflict of interest. The funders had no role in the design of the study; in the collection, analyses, or interpretation of data; in the writing of the manuscript; or in the decision to publish the results.

Appendix A: Complete Methods

A.1 Molecular Biology.

The optimized plasmid pMALc5xMBPsfGFPp60, furthermore, to be referred to as GFP-katanin was designed with maltose-binding for purification and green fluorescent protein (GFP) for visualization at the amino-terminus of the protein (Azenta Life Sciences, Chelmsford, MA). Sequence fidelity was confirmed using Sanger sequencing by Plasmidsaurus (Eugene, OR). Plasmid stocks were made for assays using outgrowth and purification instructions in Bio Basic EZ-10 Spin DNA Miniprep Kit (Markham, Ontario, CA). Plasmid should not be stored in bacteria, as that results in inactivating point-mutations in the ATPase site for katanin [18].

A.2 Protein expression and purification.

Luer-Bertani (LB) nutrient media was used for both selection plates and outgrowth media with selective antibiotic (carbenicillin) added to 100mg/L. GFP-katanin plasmid was transformed into BL21(DE3) competent *Escherichia coli* (New England BioLabs, Ipswich, MA). Transformed bacteria were grown out for one hour in SOC media (NEB) at 37°C and 250 rpm before plating on selection plates that had been pre-warmed at 37°C for one hour. Single colonies were grown on plates in a 37°C incubator for 12-16 hours. A small starter culture (5 ml) with 15-20 selected colonies was grown for two hours at 37°C and 250 rpm before inoculating the large culture and growing in the same conditions until the OD₆₀₀ reached 0.6-1.0. Induction by 1 mM Isopropyl β-D-1-thiogalactopyranoside (IPTG) for at least 16 hours at 16°C and 250 rpm was followed by purification. Cells were spun down and frozen at -80°C before pulsed sonication (20 seconds on/off for three minutes) in 15 ml Katanin Resuspension Buffer (20 mM HEPES pH 7.7, 250 mM NaCl, 0.5 mM BME, 10% glycerol, 0.25 mM ATP, 1 tablet/50ml protease inhibitors, 15 μl DNaseI). Cells were pelleted for 30 minutes at 13,000 rpm at 4°C and released protein lysate collected. Following filtration through a 0.22 μm filter, the lysate was incubated with centrifugation-washed amylose resin (NEB), and shaken on ice at 11°C at 200 rpm for one to two hours. Collection, wash and elution of the lysate and resin took place on a 5 ml poly-prep chromatography vial (Bio-Rad, Hercules, CA.) Lysate and resin were flowed through twice, then washed with four volumes (20 ml) of the Katanin Resuspension Buffer. To elute the protein from the beads, 10 mM maltose was added to Katanin Resuspension Buffer and 1 ml fractions were collected. First assessment of highest protein concentration in the fractions was performed through a dot blot assay in which droplets from each fraction were stained with Coomassie Blue (Bio-Rad) then destained with 10% acetic acid. The approximate concentration of the two best fractions from the dot blot was determined by Bradford Assay. These fractions were then drop frozen with 25% glycerol and immediately used in assays to determine katanin severing function.

A.3 Taxol-stabilized microtubule polymerization.

Rhodamine microtubule stocks with 10% rhodamine tubulin porcine mixed with 90% unlabeled porcine tubulin were hydrated from lyophilized powder (Cytoskeleton, Denver, CO) and resuspended to 5 mg/ml in PEM-100 buffer (100 mM K-PIPES pH 6.8, 2 mM MgSO₄, 2 mM EGTA). Stocks were incubated on ice for ten minutes, then spun at maximum speed for 10 minutes at 4°C. Aliquots of 15 μl were drop-frozen in liquid nitrogen. To polymerize microtubules, 1 mM GTP was added to the 10% rhodamine stock and incubated for 20 minutes at 37°C. Next, taxol was added to 50 μM for 20 minutes at 37°C to stabilize and equilibrate the microtubules. Stocks are centrifuged at 13,200 rpm for 10 minutes at room temperature, then resuspended in PEM-100 and 50 μM taxol with a Hamilton syringe to shorten microtubules. Microtubules were used for katanin severing assays within five to 10 days.

A.4. CTT peptides.

Peptides corresponding to the CTT sequences of human tubulins, and modified forms, were custom synthesized and obtained from Peptide 2.0 (Chantilly, VA). Purity and sequence accuracy were confirmed by mass spectrometry performed by Dr. Lisa Jenkins, NCI, NIH.

Tubulin Carboxy-terminal tail (CTT) peptides were provided by Dan Sackett in 7-10 mM stocks and stored at -80°C. The CTT sequences can be found in Table 1.

2.5 *In vitro* microtubule severing assays.

Flow chambers with 10 μ l channels were made by adhering double-stick tape (3M, St. Paul, MN) to a microscope slide and attaching a silanized coverslip cross-wise. Silanized coverslips were UVO sterilized, cleaned with rinses of acetone, ethanol, 0.1 M KOH and ddH₂O before coating with PlusOne Repel-Silane 2% dimethyldichlorosilane (Cytiva, Marlborough, MA). Samples were made in the chambers by flowing through the chamber using a pipette and filter paper to wick from the other side. For severing assays, we first flowed 5% MAB1864 tubulin YL $\frac{1}{2}$ antibody (Merck-Millipore, Billerica, MA) in PEM-100 for three minutes to provide a binding site for microtubules. Second, we flowed 5% (w/v) Pluronic F127 to act as a polymer brush to block the surface, allowing three minutes for incubation. Next, we flowed 10% rhodamine-labeled microtubules diluted 1:100 (final tubulin concentration 454 nM) and allowed them to adhere for three minutes. During the incubation, an aliquot of katanin was rapidly defrosted from -80°C and diluted to assay concentration. The chamber was then washed with Katanin Activity Buffer (20 mM HEPES pH 7.7, 10% glycerol, 2 mM MgCl₂, 2 mM ATP, 0.025 mg/ml BSA, 0.05% F127, 10 mM dithiothreitol (DTT), 15 mg/ml glucose, 0.15 mg/ml catalase, 0.05 mg/ml) to remove excess unadhered microtubules. The chamber was then situated on the microscope to find a good field for the assay before flowing Katanin Activity Buffer with GFP-katanin and CTT tails at their respective concentrations.

Imaging was performed using epifluorescence and total internal reflection (TIRF) with a home-built laser illumination system around a Nikon Ti-E microscope (Nikon USA, Melville, NY). Epifluorescence was used to image rhodamine microtubules in the red channel, and TIRF was used to image GFP-katanin illuminating with a 488 nm laser. Images were collected with a 60x, oil-coupled TIRF objective with a numerical aperture of 1.49 (Nikon USA, Melville, NY). The two-color imaging was performed using shuttering the red channel (400-800 ms exposure) and green channel (70-200 ms exposure) sequentially. The 5-minute movies recorded with 3 second intervals using Nikon Elements software (Nikon USA, Melville, NY) driving an Ixon EMCCD camera (Andor, Belfast, Northern Ireland) with a final pixel size of 160 nm. Movie data was saved as a 16-bit time series as nd2 files with metadata. Movies were started recording before the GFP-katanin mixture was flowed while imaging. After the 5 minutes, a new field of view was imaged to ensure that the loss of microtubule polymer was universal in the chamber and not due to imaging conditions.

Each of the 64 treatments were run two to three times for replication and for obtaining 15-20 MTs for analysis. Four control chambers were run each day to ensure chamber activity was caused by the respective treatment conditions. The microtubules only control demonstrates the intrinsic depolymerization that occurs due to imaging conditions. Next, the concentration needed to sever microtubules within 2-3 minutes is determined in the presence of ATP. Once the optimal katanin concentration is determined, the assay is repeated in the absence of ATP to again test the imaging conditions in the presence of a GFP-katanin binding to microtubules. Finally, the beta CTT is used as a positive inhibition control daily to ensure that the chamber can be inhibited by 2 μ M of beta tubulin CTT. Each of the 12 CTT peptides was assayed using five different concentrations (0, 0.5, 0.75, 1, 1.5, 2 μ M) to observe the ability of GFP-katanin to sever.

2.6 *Quantifying Microtubule Loss of Polymer and GFP-katanin Binding*

Nikon nd2 image files were opened in FIJI and the two color channels split to view microtubule and GFP-katanin data separately. Each channel was drift-corrected using the StackReg tool set to translation. A single frame from the movie was saved separately to identify the regions of interest (ROIs) that were used for analysis. Individual microtubules were selected using the segmented line tool. The mean intensity of each microtubule was measured using a 3-pixel wide ROI on the microtubule of the drift-corrected movie using the measure stacks tool to measure the same line over the image series. The same ROI was shifted 5 pixels away from the microtubule and the stack was measured again to obtain

the background intensity data. Only single microtubules (not bundles) were selected based on minimum size and representative position.

The mean intensity of the microtubule (signal) was divided by the mean intensity of the background (noise) then subtracted by 1 to remove the background. The microtubule channel was further normalized to the first frame in focus after GFP-katanin was flowed into the chamber, setting this initial value to 1 (100%) so that subsequent measurements record the percentage of the polymer that remained throughout the movie. At least 10-20 microtubules were measured on at least 2 distinct chambers per CTT. The reported percentage of polymer remaining over time was an average of all the microtubules measured at the same conditions. The error bars represent the standard error of the mean. The number of microtubules in each average data set are given in the figures.

For each condition, the microtubule loss of polymer was plotted against the time of the movie and fit to an fast exponential decay of the form: $M(t) = M(\infty) + A \exp(-t/\tau)$, where $M(t)$ is the percentage of microtubule polymer at time t , $M(\infty)$ is the final amount of polymer at the end of the movie (for many data sets this was 0), A is the amplitude of the exponential decay, and τ is the characteristic decay time. For decays where the characteristic time was longer than the movie time, we used a linear approximation to the exponential decay and fit the data to this form: $M(t) = A(1 - x/\tau)$. This form does not have an offset because it would not be possible to determine. The fit parameters and uncertainty of the fit was recorded and reported in the figures.

The intensity of the GFP-katanin binding to microtubules over time was measured the same way as the microtubule channel, except the data was not normalized from the first frame. Instead the average intensity was compared to the same day control with no CTT added. An average maximum data was determined from plots of the GFP-katanin intensity over time for each experimental condition. For each CTT, the GFP intensity data was normalized so that the 0 CTT data for the same day had a maximum of 1. The normalized GFP intensity values are reported in the figures. appendix.

References

1. Brouhard, G.J.; Rice, L.M. Microtubule Dynamics: An Interplay of Biochemistry and Mechanics. *Nat. Rev. Mol. Cell Biol.* **2018**, *19*, 451–463, doi:10.1038/s41580-018-0009-y.
2. Verhey, K.J.; Gaertig, J. The Tubulin Code. *Cell Cycle* **2007**, *6*, 2152–2160.
3. Yu, I.; Garnham, C.P.; Roll-Mecak, A. Writing and Reading the Tubulin Code. *J Biol Chem* **2015**, *290*, 17163–17172, doi:10.1074/jbc.R115.637447.
4. Janke, C.; Kneussel, M. Tubulin Post-Translational Modifications: Encoding Functions on the Neuronal Microtubule Cytoskeleton. *Trends Neurosci.* **2010**, *33*, 362–372.
5. Janke, C.; Magiera, M.M. The Tubulin Code and Its Role in Controlling Microtubule Properties and Functions. *Nat. Rev. Mol. Cell Biol.* **2020**, *21*, 307–326, doi:10.1038/s41580-020-0214-3.
6. Bodakuntla, S.; Jijumon, A.S.; Villablanca, C.; Gonzalez-Billault, C.; Janke, C. Microtubule-Associated Proteins: Structuring the Cytoskeleton. *Trends Cell Biol.* **2019**, *29*, 804–819, doi:10.1016/j.tcb.2019.07.004.
7. Sharp, D.J.; Ross, J.L. Microtubule-Severing Enzymes at the Cutting Edge. *J Cell Sci* **2012**, *125*, 2561–2569, doi:10.1242/jcs.101139.
8. Roll-Mecak, A.; McNally, F.J. Microtubule-Severing Enzymes. *Curr Opin Cell Biol* **2010**, *22*, 96–103, doi:10.1016/j.ceb.2009.11.001.
9. Lynn, N.A.; Martinez, E.; Nguyen, H.; Torres, J.Z. The Mammalian Family of Katanin Microtubule-Severing Enzymes. *Front. Cell Dev. Biol.* **2021**, *9*, 692040, doi:10.3389/fcell.2021.692040.
10. Hartman, J.J.; Mahr, J.; McNally, K.; Okawa, K.; Iwamatsu, A.; Thomas, S.; Cheesman, S.; Heuser, J.; Vale, R.D.; McNally, F.J. Katanin, a Microtubule-Severing Protein, Is a Novel AAA ATPase That Targets to the Centrosome Using a WD40-Containing Subunit. *Cell* **1998**, *93*, 277–287, doi:10.1016/S0092-8674(00)81578-0.
11. Joly, N.; Martino, L.; Gigant, E.; Dumont, J.; Pintard, L. Microtubule-Severing Activity of AAA-ATPase Katanin Is Essential for Female Meiotic Spindle Assembly. *Development* **2016**, dev.140830, doi:10.1242/dev.140830.

12. Nithianantham, S.; McNally, F.J.; Al-Bassam, J. Structural Basis for Disassembly of Katanin Heterododecamers. *J. Biol. Chem.* **2018**, *293*, 10590–10605, doi:10.1074/jbc.RA117.001215.
13. Faltova, L.; Jiang, K.; Frey, D.; Wu, Y.; Capitani, G.; Prota, A.E.; Akhmanova, A.; Steinmetz, M.O.; Kammerer, R.A. Crystal Structure of a Heterotetrameric Katanin P60:P80 Complex. *Structure* **2019**, *27*, 1375–1383.e3, doi:10.1016/j.str.2019.07.002.
14. Hartman, J.J.; Vale, R.D. Microtubule Disassembly by ATP-Dependent Oligomerization of the AAA Enzyme Katanin. *Science* **1999**, *286*, 782–785.
15. Eckert, T.; Le, D.T.-V.; Link, S.; Friedmann, L.; Woehlke, G. Spastin's Microtubule-Binding Properties and Comparison to Katanin. *PLoS One* **2012**, *7*, e50161, doi:10.1371/journal.pone.0050161.
16. Zhang, D.; Grode, K.D.; Stewman, S.F.; Diaz-Valencia, J.D.; Liebling, E.; Rath, U.; Riera, T.; Currie, J.D.; Buster, D.W.; Asenjo, A.B.; et al. Drosophila Katanin Is a Microtubule Depolymerase That Regulates Cortical-Microtubule plus-End Interactions and Cell Migration. *Nat Cell Biol* **2011**, *13*, 361–370, doi:10.1038/ncb2206.
17. Díaz-Valencia, J.D.; Morelli, M.M.; Bailey, M.; Zhang, D.; Sharp, D.J.; Ross, J.L. Drosophila Katanin-60 Depolymerizes and Severs at Microtubule Defects. *Biophys. J.* **2011**, *100*, 2440–2449, doi:10.1016/j.bpj.2011.03.062.
18. Bailey, M.E.; Sackett, D.L.; Ross, J.L. Katanin Severing and Binding Microtubules Are Inhibited by Tubulin Carboxy Tails. *Biophys J* **2015**, *109*, 2546–2561, doi:10.1016/j.bpj.2015.11.011.
19. Belonogov, L.; Bailey, M.E.; Tyler, M.A.; Kazemi, A.; Ross, J.L. Katanin Catalyzes Microtubule Depolymerization Independently of Tubulin C-terminal Tails. *Cytoskeleton* **2019**, *76*, 254–268, doi:10.1002/cm.21522.
20. Whitehead, E.; Heald, R.; Wilbur, J.D. N-Terminal Phosphorylation of P60 Katanin Directly Regulates Microtubule Severing. *J Mol Biol* **2013**, *425*, 214–221, doi:10.1016/j.jmb.2012.11.022.
21. Loughlin, R.; Wilbur, J.D.; McNally, F.J.; Nédélec, F.J.; Heald, R. Katanin Contributes to Interspecies Spindle Length Scaling in *Xenopus*. *Cell* **2011**, *147*, 1397–1407, doi:10.1016/j.cell.2011.11.014.
22. Valenstein, M.L.; Roll-Mecak, A. Graded Control of Microtubule Severing by Tubulin Glutamylation. *Cell* **2016**, *164*, 911–921, doi:10.1016/j.cell.2016.01.019.
23. Szczesna, E.; Zehr, E.A.; Cummings, S.W.; Szyk, A.; Mahalingan, K.K.; Li, Y.; Roll-Mecak, A. Combinatorial and Antagonistic Effects of Tubulin Glutamylation and Glycylation on Katanin Microtubule Severing. *Dev. Cell* **2022**, *57*, 2497–2513.e6, doi:10.1016/j.devcel.2022.10.003.
24. Vale, R.D. Severing of Stable Microtubules by a Mitotically Activated Protein in *Xenopus* Egg Extracts. *Cell* **1991**, *64*, 827–839.
25. Wehenkel, A.; Janke, C. Towards Elucidating the Tubulin Code. *Nat. Cell Biol.* **2014**, *16*, 303–305, doi:10.1038/ncb2938.
26. Maliekal, T.T.; Dharmapal, D.; Sengupta, S. Tubulin Isoforms: Emerging Roles in Defining Cancer Stem Cell Niche. *Front. Immunol.* **2022**, *13*, 876278, doi:10.3389/fimmu.2022.876278.
27. Wimley, W.C.; White, S.H. Experimentally Determined Hydrophobicity Scale for Proteins at Membrane Interfaces. *Nat. Struct. Mol. Biol.* **1996**, *3*, 842–848, doi:10.1038/nsb1096-842.
28. Jiang, K.; Rezabkova, L.; Hua, S.; Liu, Q.; Capitani, G.; Altelaar, A.F.M.; Heck, A.J.R.; Kammerer, R.A.; Steinmetz, M.O.; Akhmanova, A. Microtubule Minus-End Regulation at Spindle Poles by an ASPM-Katanin Complex. *Nat Cell Biol* **2017**, *19*, 480–492, doi:10.1038/ncb3511.
29. Vemu, A.; Szczesna, E.; Zehr, E.A.; Spector, J.O.; Grigorieff, N.; Deaconescu, A.M.; Roll-Mecak, A. Severing Enzymes Amplify Microtubule Arrays through Lattice GTP-Tubulin Incorporation. *Science* **2018**, *361*, eaau1504, doi:10.1126/science.aau1504.
30. Gundersen, G.G.; Bulinski, J.C. Distribution of Tyrosinated and Nontyrosinated Alpha-Tubulin during Mitosis. *J Cell Biol* **1986**, *102*, 1118–1126.
31. Gundersen, G.G.; Khawaja, S.; Bulinski, J.C. Generation of a Stable, Posttranslationally Modified Microtubule Array Is an Early Event in Myogenic Differentiation. *J Cell Biol* **1989**, *109*, 2275–2288.
32. Khawaja, S.; Gundersen, G.G.; Bulinski, J.C. Enhanced Stability of Microtubules Enriched in Detyrosinated Tubulin Is Not a Direct Function of Detyrosination Level. *J. Cell Biol.* **1988**, *106*, 141–149, doi:10.1083/jcb.106.1.141.

33. Chen, J.; Kholina, E.; Szyk, A.; Fedorov, V.A.; Kovalenko, I.; Gudimchuk, N.; Roll-Mecak, A. α -Tubulin Tail Modifications Regulate Microtubule Stability through Selective Effector Recruitment, Not Changes in Intrinsic Polymer Dynamics. *Dev. Cell* **2021**, *56*, 2016–2028.e4, doi:10.1016/j.devcel.2021.05.005.
34. Peris, L.; Wagenbach, M.; Lafanechère, L.; Brocard, J.; Moore, A.T.; Kozielski, F.; Job, D.; Wordeman, L.; Andrieux, A. Motor-Dependent Microtubule Disassembly Driven by Tubulin Tyrosination. *J Cell Biol* **2009**, *185*, 1159–1166, doi:10.1083/jcb.200902142.
35. Chew, S.; Balasubramanian, R.; Chan, W.-M.; Kang, P.B.; Andrews, C.; Webb, B.D.; MacKinnon, S.E.; Oystreck, D.T.; Rankin, J.; Crawford, T.O.; et al. A Novel Syndrome Caused by the E410K Amino Acid Substitution in the Neuronal β -Tubulin Isotype 3. *Brain* **2013**, *136*, 522–535, doi:10.1093/brain/aws345.
36. Tischfield, M.A.; Baris, H.N.; Wu, C.; Rudolph, G.; Van Maldergem, L.; He, W.; Chan, W.-M.; Andrews, C.; Demer, J.L.; Robertson, R.L.; et al. Human TUBB3 Mutations Perturb Microtubule Dynamics, Kinesin Interactions, and Axon Guidance. *Cell* **2010**, *140*, 74–87, doi:10.1016/j.cell.2009.12.011.
37. Latremoliere, A.; Cheng, L.; DeLisle, M.; Wu, C.; Chew, S.; Hutchinson, E.B.; Sheridan, A.; Alexandre, C.; Latremoliere, F.; Sheu, S.-H.; et al. Neuronal-Specific TUBB3 Is Not Required for Normal Neuronal Function but Is Essential for Timely Axon Regeneration. *Cell Rep* **2018**, *24*, 1865–1879.e9, doi:10.1016/j.celrep.2018.07.029.
38. Yigit, G.; Wieczorek, D.; Bögershausen, N.; Beleggia, F.; Möller-Hartmann, C.; Altmüller, J.; Thiele, H.; Nürnberg, P.; Wollnik, B. A Syndrome of Microcephaly, Short Stature, Polysyndactyly, and Dental Anomalies Caused by a Homozygous KATNB1 Mutation. *Am J Med Genet A* **2016**, *170*, 728–733, doi:10.1002/ajmg.a.37484.
39. Mishra-Gorur, K.; Çağlayan, A.O.; Schaffer, A.E.; Chabu, C.; Henegariu, O.; Vonhoff, F.; Akgümüş, G.T.; Nishimura, S.; Han, W.; Tu, S.; et al. Mutations in KATNB1 Cause Complex Cerebral Malformations by Disrupting Asymmetrically Dividing Neural Progenitors. *Neuron* **2014**, *84*, 1226–1239, doi:10.1016/j.neuron.2014.12.014.
40. Zheng, J.; Long, F.; Cao, X.; Xiong, B.; Li, Y. Knockout of *Katnal2* Leads to Autism-like Behaviors and Developmental Delay in Zebrafish. *Int. J. Mol. Sci.* **2022**, *23*, 8389, doi:10.3390/ijms23158389.
41. Waibl, F.; Fernández-Quintero, M.L.; Wedl, F.S.; Kettenberger, H.; Georges, G.; Liedl, K.R. Comparison of Hydrophobicity Scales for Predicting Biophysical Properties of Antibodies. *Front. Mol. Biosci.* **2022**, *9*, 960194, doi:10.3389/fmolb.2022.960194.
42. Kovacs, J.M.; Mant, C.T.; Hodges, R.S. Determination of Intrinsic Hydrophilicity/Hydrophobicity of Amino Acid Side Chains in Peptides in the Absence of Nearest-Neighbor or Conformational Effects. *Biopolymers* **2006**, *84*, 283–297, doi:10.1002/bip.20417.
43. Schaedel, L.; John, K.; Gaillard, J.; Nachury, M.V.; Blanchoin, L.; Théry, M. Microtubules Self-Repair in Response to Mechanical Stress. *Nat Mater* **2015**, *14*, 1156–1163, doi:10.1038/nmat4396.
44. Srayko, M.; O'toole, E.T.; Hyman, A.A.; Müller-Reichert, T. Katanin Disrupts the Microtubule Lattice and Increases Polymer Number in *C. Elegans* Meiosis. *Curr Biol* **2006**, *16*, 1944–1949, doi:10.1016/j.cub.2006.08.029.